Energetic Ion Production and Keeper Erosion in Hollow Cathode Discharges

IEPC-2005-266

Presented at the 29th International Electric Propulsion Conference, Princeton University, October 31 – November 4, 2005

Dan M. Goebel*, Kristina Jameson†, Ira Katz‡, Ioannis G. Mikellides§
Jet Propulsion Laboratory, California Institute of Technology, Pasadena, CA 91109

Abstract: Ions with energies significantly in excess of the discharge voltage have been reported in high current hollow cathode discharges for many years. Models of DC potential hills downstream of the cathode and ion acoustic instabilities in a double layer postulated in the cathode orifice have been proposed to explain these energetic ions, but have not been substantiated by experiments. An investigation of the DC and rf density and potential profiles measured throughout the discharge by fast miniature scanning probes suggests that ionization instabilities and turbulent oscillations at the edge of the characteristic "plasma ball" observed downstream of the cathode orifice are responsible for both the energy and spatial distribution of the energetic ions. Keeper erosion rates and wear profiles are discussed with respect to the production of these high-energy ions.

I. Introduction

Hollow cathodes have been used in a multitude of applications to produce plasma for ion sources, lasers, plasma processing, etc. The primary purpose of enclosing the electron emitter inside a hollow structure and extracting electrons from the cathode plasma through an orifice is to protect the thermionic emitter from energetic ion bombardment that can degrade the work function of the surface[1]. The hollow cathode is also often enclosed inside another electrode called the keeper that is a biased hollow tube with a slightly larger orifice aligned with the cathode aperture. The purpose of the keeper is to draw a small amount of current from the cathode to facilitate turn-ON, to maintain the cathode temperature if the main discharge current is turned off or interrupted, and to protect the cathode orifice plate and heater from ion bombardment and erosion.

With sufficient gas flow, orificed thermionic hollow cathodes can produce quiescent discharges at modest currents of amperes to ten's of amperes. However, as the discharge current is increased for a given cathode orifice size and gas flow rate, the noise in the discharge voltage and probe signals from the plasma increases, and the cathodes produce ions with energies significantly in excess of the discharge voltage[2-6]. Cathode orifice plate and keeper electrode erosion rates measured or inferred in various experiments[7,8] and in ion thruster life tests[9-11] have been found to be much higher than anticipated. These results have been attributed to the high-energy ions bombarding and sputtering the cathode electrodes. Of particular concern is the apparent change in the erosion characteristics at different discharge power levels in the NSTAR ion thruster[12] Extended Life Test (ELT)[10] that caused the keeper to entirely erode away in less than 15,000 hours. The source and characteristics of these high-energy ions has been a subject of much research and debate. Models of a DC potential hill[13] located inside or just downstream of the cathode orifice, or ion acoustic instabilities in a double layer postulated in the orifice of the

* Principal Scientist, Jet Propulsion Laboratory, dan.m.goebel@jpl.nasa.gov
† Graduate Student, University of California, Los Angeles, kristina.k.jameson@jpl.nasa.gov
‡ Group Supervisor, Advanced Propulsion Group, Jet Propulsion Laboratory, ira.katz@jpl.nasa.gov
§ Senior Engineer, Jet Propulsion Laboratory, Ioannis.G.Mikellides@jpl.nasa.gov

cathode[2], have been proposed to explain the production of these ions. However, there have been no direct measurements in probe studies to date[14-16] of potential hills or unstable double layers at the cathode orifice or in the cathode plume that might explain the mechanisms responsible for the high-energy ions or the electrode wear rates and patterns.

To investigate this issue, the hollow cathode test facility[14] at JPL was instrumented with an array of scanning probes and a 4-grid retarding potential analyzer (RPA). The probes are very small (0.5-mm-dia. ceramic tubes) to avoid perturbing the plasma, and are scanned pneumatically at speeds of up to 2 m/sec to avoid melting in the high-density plasmas found in the cathode and keeper regions. A standard 1/4" NSTAR cathode was installed in a conical-to-cylindrical anode that approximates the NSTAR ion thruster geometry and operated at various throttle levels. In addition, a 1.5-cm diameter NEXIS ion thruster[17] hollow cathode was also installed in the facility and tested to determine the effect of cathode size and current scaling on the keeper erosion physics.

The experiments detected relatively few ions with energies higher than the discharge voltage flowing downstream from the cathode on axis, but found a significant amount of high-energy ions for some discharge conditions traveling in the radial direction from the characteristic plasma ball observed in front of the cathode. A high speed scanning emissive probe capable of measuring the rf plasma potential directly in front of the cathode detected significant plasma oscillations in the ion acoustic range from the edge of the plasma ball near the cathode exit. A detailed investigation of the DC and rf density and potential profiles measured throughout the hollow cathode discharge by the scanning probes indicates that there is no DC potential hill at or near the cathode orifice. In the orifice, a potential discontinuity or double layer with a magnitude of less than 10 V has been detected that has ion-acoustic type oscillations on the order of 1 MHz, but these are small in amplitude ($\delta n/n \approx 1\%$). Outside the keeper, the plasma potential forms a well or trough centered on the high density "plasma ball" observed there, with the potential increasing axially over several cm to a peak value near the discharge voltage and radially to potentials 5 to 10 V in excess of the discharge voltage that extend to near the anode surface. Measurements of the plasma potential fluctuations with an emissive probe constructed to be sensitive to up to 1 MHz show large amplitude fluctuations (> 50 V) in the plasma potential ranging from 60 to 500 kHz starting at the edge of the ball and extending radially outward to the wall. The collected current by the RPA is correlated to the density and potential fluctuations measured by the probes. The plasma potential fluctuations are found to be small in the axial direction, and do not extend into the cathode. In the radial direction, the potential fluctuations can exceed five times T_e, suggesting turbulent acoustic oscillations and/or ionization instabilities near the edge of the "plasma ball" are responsible for both the high energy and spatial distribution of the energetic ions. The axial location of the plasma ball is observed to change with the throttle level, with the NSTAR TH8 setting pulling the ball back into the keeper orifice. This may explain the rapid radial erosion of the keeper observed at this setting due to the primarily radially directed high-energy ions directly bombarding the keeper orifice inside diameter. In this paper, the plasma parameter and ion energy measurements from the scanning probes and RPA will be presented for the two cathodes with discussion of the impact on keeper erosion.

II. Experimental Arrangement

The JPL hollow cathode test facility[14] was instrumented with an array of scanning probes and a 4-grid retarding potential analyzer (RPA), as illustrated in Fig. 1. Two hollow cathodes were investigated in these experiments. The first is a conventional NSTAR-size cathode[1] with a 6.35-mm diameter molybdenum-rhenium tube with a 1-mm diameter orifice. A porous tungsten emitter impregnated with a low-work-function barium-calcium-aluminate mixture is located inside the cathode. Electrons emitted from the insert by field-enhanced thermionic emission generate a cathode-plasma inside the insert region, from which electrons are extracted through the orifice to generate the plasma in the discharge chamber. The cathode is heated by a standard sheathed heater, which is turned off during discharge operation. A keeper electrode made from molybdenum or graphite fully encloses the cathode, and the keeper orifice is about 4.6 times the diameter of the cathode orifice. The second cathode is a conventional barium impregnated tungsten insert in a 1.5 cm dia. molybdenum tube with a tungsten orifice plate e–beam welded on the end. The cathode is heated by a standard sheathed heater, which is turned off during discharge operation. The NEXIS graphite keeper electrode also fully encloses the cathode, and the keeper orifice is about 1.7 times the diameter of the cathode orifice.

The cathode and scanning probe system are mounted on an 8" Conflat flange installed in one port of 0.75-m diameter, 2-m long vacuum chamber. The chamber is pumped by two 10" CTI cryopumps with a combined xenon pumping speed of 1275 l/sec for xenon. The base pressure of the chamber is in the 1×10^{-8} Torr range, and during

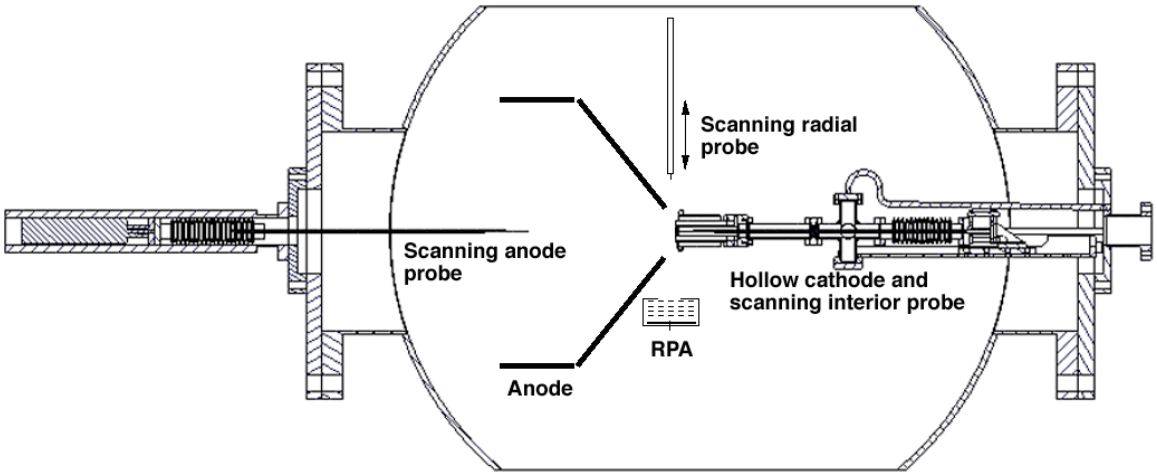

Figure 1. Schematic drawing of the experimental layout showing the cathode, anode, three scanning probe diagnostics and the retarding-potential analyzer (RPA) which could be located radially (shown) or axially from the cathode.

normal operation about 5 sccm of xenon flow the chamber pressure remains in the low 10^{-5} Torr range, where the xenon gas is controlled and measured by a digital MKS mass flow controller. Additionally, a precision Baratron capacitive manometer is used to measure the pressure in the hollow cathode during operation, data from which has been reported elsewhere[14,15].

The cathode and scanning probe assembly mounted in the vacuum system are shown in Figure 2a. The experimental arrangement uses a water-cooled anode that has a conical section and a cylindrical section approximately 30 cm in diameter with an NSTAR-like magnetic field arrangement. The scanning probe inside the cathode insert region has a 0.5 mm diameter alumina tube with a 0.127 mm diameter tungsten wire electrode that protrudes from the small-bore ceramic tubing a distance of 0.25 mm. Even though the wire electrode is keep at a minimal length for electron collection, the probe has collected up to 5 A of current in the high density region near the orifice of the cathode. The cathode probe is aligned axially in the system by two slide-guides internal to the cathode system. The probe has a linear throw of 4 cm and can traverse the cathode at one to two meters per second with a resolution of 0.25 mm. A dual bellows system in the cathode assembly is used to keep constant volume inside the cathode assembly, which maintains a constant pressure in the cathode while the Langmuir probe is being inserted into and out of the insert region. With the NSTAR cathode installed, the cathode probe occupies about 25% of the cathode orifice cross sectional area, and significantly perturbs the plasma discharge if the probe is pushed too far past the upstream orifice entrance. For this reason, data is only taken prior to the probe entering the cathode orifice. With the larger NEXIS cathode, inserting the probe into the orifice does not significantly perturb the discharge, and plasma parameters in the cathode orifice and

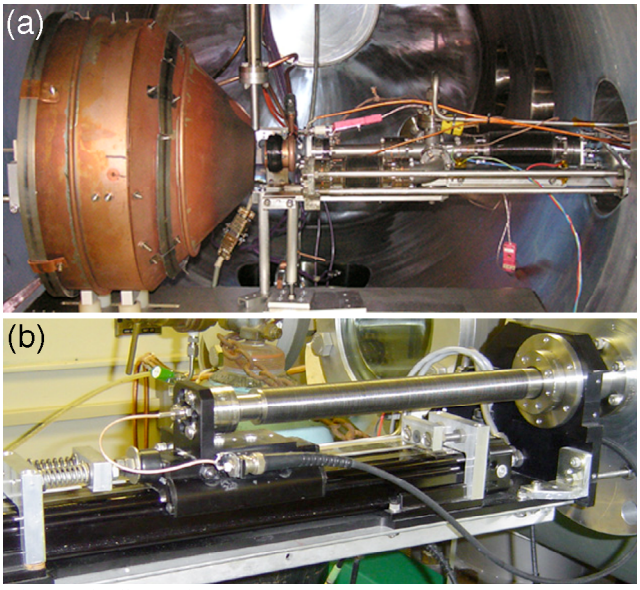

Figure 2. Scanning probe assemblies (a) cathode probe mounted in the vacuum chamber with the conical-to-cylindrical water cooled anode with ring-cusp magnets, and (b) the anode probe drive system outside the vacuum system showing the high speed pneumatic plunger and bellows arrangement.

keeper region can be measured. Also shown in Fig. 2a is a solenoid coil wound on a water cooled cylinder directly around the cathode to provide an axial magnetic field of adjustable amplitude at the cathode exit that simulates the cathode field in ring-cusp thrusters. Reference 14 contains a full description of the cathode probe assembly and test facility.

The anode scanning-probe assembly is shown in Figure 2b, where the pneumatic plunger and vacuum bellows arrangement mounted on the outside of the vacuum system are seen. The diameter of the ceramic tubing interior to the vacuum system is stepped down from 3 mm to 0.5 mm diameter for the 3cm section that is inserted deepest into the plasma in order to minimize perturbation to the plasma in the anode region. The exposed electrode is again a 0.127 mm tungsten wire, but has a length of 1.3 mm to collect sufficient current away from the keeper region to accurately determine the plasma parameters. The anode probe has nearly three times the throw of the cathode probe and 5 times the unsupported length so as to not perturb the anode-plasma, and also moves at one meter a second with a position resolution of 0.5 mm. Very careful iterative alignment techniques are used to ensure that the anode probe is aligned with the cathode orifice and within 0.5 mm of the centerline. The anode probe can be fully inserted into the keeper orifice, although whip of the long ceramic sometimes causes the tip to touch the keeper or cathode during retraction.

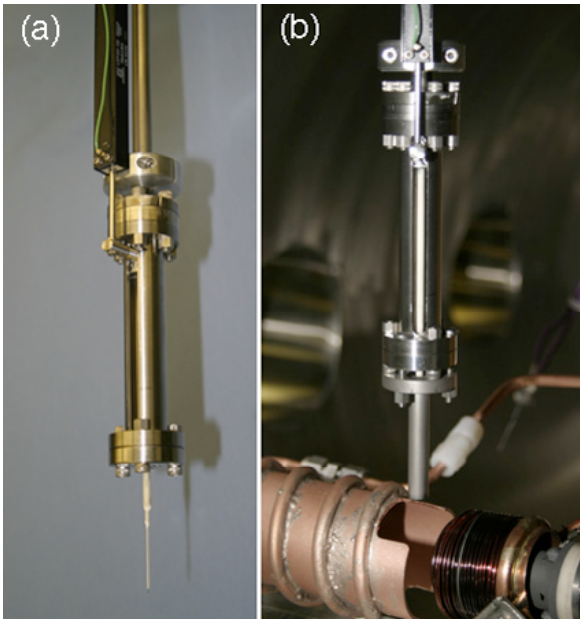

Figure 3. Transverse scanning probe with position transducer (a), and being tested with NSTAR cathode and small cylindrical anode (b).

The radially scanning emissive probe is shown in Figure 3. It uses a pneumatic plunger mounted external to the vacuum system, identical to the cathode plunger arrangement, and is mounted to a Huntington X-Y manipulator outside the vacuum system to provide positioning relative to the keeper exit point. The radial probe has a linear throw of 4 cm, also at one meter per second, and is aligned by a slide-guide internal to the vacuum system to obtain a position resolution of 0.25 mm. The probe can be positioned in front of the keeper as close as 1 mm out to 2.5 cm downstream. The probe tip is a 0.127 mm diameter tungsten hair-pin wire feed through two side-by-side 0.5 mm diameter alumina tubes. A floating 5-ampere power supply provides the current to heat the tungsten wire electrode to emit electrons. The probe signal fed to a high impedance, high frequency circuit and a buffer amplifier to detect any oscillations present in the signal. When the emissive probe is not in use, it is pulled back into a 6.5-mm-dia. tube that is positioned sufficiently out of the discharge plume to protect it from ion bombardment.

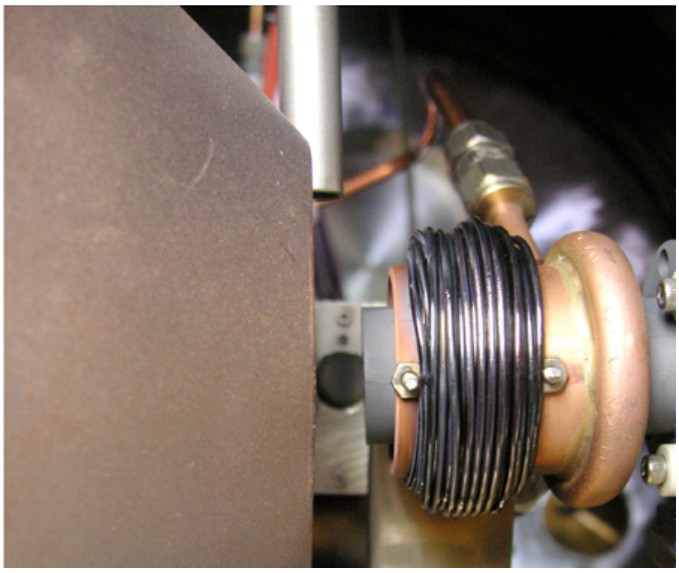

Figure 4. Photograph of the NSTAR cathode, conical anode, RPA in the background, and transverse probe coming in from the top.

A gridded retarding potential analyzer is used to determine the ion energy distribution. A four-grid arrangement was used where the first grid in contact with the plasma floats, the second grid is biased to repel electrons, and only the ions with energy greater than potential applied to the dual-discriminator grid can pass through and reach the collector. A photograph of the RPA positioned radially from the gap between the anode and the keeper is shown in Fig. 4. However, the RPA could also be moved on axis to obtain axial

energy distributions downstream from the cathode. In this case, the anode probe assembly is removed from the chamber to allow the RPA to be placed unobstructed on axis at the exit of the anode.

Experiments are conducted with a NSTAR like anode with a diverging conical section followed by a straight cylindrical section, constructed of copper and water cooled. The anode can be seen in Fig. 2a and the entrance where the cathode was placed is seen clearly in Fig. 4. The conical section has a minimum diameter of approximately 5 cm, and is joined to the 30-cm-dia. straight cylindrical section. The gap between the cathode keeper exit and anode is adjustable, and is typically about 2 cm to allow for visualization of the cathode plume and to acquire radial RPA traces. A solenoid coil positioned around the cathode produces an axial magnetic field at the cathode orifice, which couples to two rings of permanent magnets around the anode body to simulate the NSTAR magnetic field geometry. This anode geometry is capable of reproducing the full NSTAR throttle table, producing discharges at 6.1 A at 26.8 V representing TH4, 8.2 A at 26 V representing TH8, 10.9 V at 26.2 V representing TH12, and 13.1 A and 25.2 V representing TH15.

The bias voltage applied to the probe tips is generated by a programable waveform synthesizer that drives a Kepco bipolar power supply. The voltage waveform is typically a sawtooth ramp that scans from –10 to + 50 V in the anode region and from -10 to +20 in the cathode region in a time of 1 msec. When using the NSTAR cathode, the cathode probe can only be swept once per insertion to avoid overheating the probe tip in the very high-density plasma ($>10^{15}$ cm^{-3} density) near the hollow cathode orifice. A delay generator is used to take consecutive traces allowing the cathode plasma parameters can be mapped. The NEXIS cathodes has nearly an order of magnitude lower pressure inside and corresponding lower plasma density, so that multiple voltage sweeps can be made during the probe insertion to map-out the plasma profiles with a single scan. Electron temperatures and plasma potentials are determined in less than half of the total 1 msec trace, therefore the position uncertainty for the plasma parameters is on the order of 0.5 mm over most of the scan and less than 0.25 mm near the full insertion point. The probe position, voltage and current data is collected on a PC at a sample rate of 300 kHz, resulting in 300 data points in each probe characteristic curve. The plasma potential and electron temperatures are found by classical Langmuir probe analysis[16]. The electron temperature is found by fitting an exponential curve to the electron retardation region of the Langmuir trace. The electron temperatures have error bars about 0.5 V and the plasma potentials have error bars of ±1 V in the cathode region and up to ± 2V in the anode region. Recently, electron energy distribution functions have been measured external to the cathode using both a second derivative technique and an rf-second harmonic technique, but these will not be described here.

III. NSTAR Cathode Results

The NSTAR thruster is normally operated over a wide range of parameters described in a "throttle table", which is designed to keep the discharge voltage at about 25 V while the discharge current and/or gas flow rate is changed to produce different thrust levels.[12] In these experiments, we operated primarily at four throttle conditions (TH15, 12, 8 and 4), with the majority of time investigating the performance in the high power TH15 and mid-power TH8 modes where the keeper erosion data is extensive. The keeper erosion in the NSTAR thruster represents a significant potential failure mechanism. Figure 5 shows a cross section of the keeper electrode after the 8200 hour Long Duration Test (LDT)[9] at JPL. In this test, the thruster was operated at the highest power level, TH15, corresponding to 2.3 kW of total thruster power and a discharge current of 13 A at about 25 V. The molybdenum keeper downstream face was significantly eroded during the test, indicating significant ion bombardment of the keeper surface. The face of a graphite keeper on the NSTAR cathode that was run in the test facility for less than 20 hours at TH15 is shown in Figure 7. While there is no significant erosion of the graphite during this test because of its low sputtering yield, the surface discolorization shows the ion bombardment in the same region radially away from the cathode orifice. This keeper face erosion was identified after the LDT

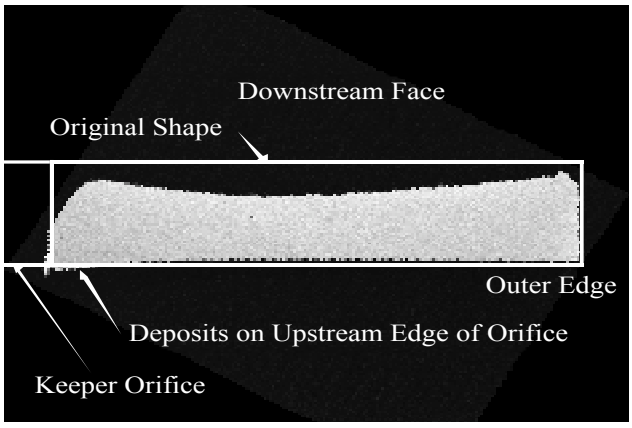

Figure 5. NSTAR keeper cross section after the 8200 hour LDT test at TH15 showing significant erosion of the keeper face.

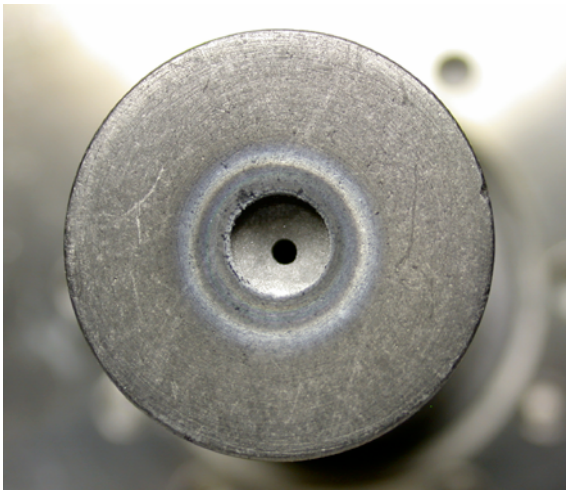

Figure 6. Graphite keeper face discoloration showing ion bombardment pattern for approximately 20 hours of operation at TH15.

as a significant life risk for the thruster. However, sequential photographs of the keeper electrode during the 30,000-hour ELT[10] life test showed that the keeper eroded significantly faster during operation at the TH8 throttle level, and the keeper orifice diameter increased with time. Figure 6 shows photographs of the NSTAR cathode assembly at the several times during the first 16,000 hours of the ELT test, illustrating the complete sputter erosion removal of the keeper electrode. The reason for this high erosion in the lower power TH8 throttle mode has not been explained even by independent tests of the wear rates by surface layer activation[16].

A. NSTAR Cathode Plasma Data

To attempt to understand the keeper erosion mechanisms, we measured the complete axial and radial profiles of the plasma density, potential and electron temperature in the cathode and keeper regions. Analysis of the plasma parameters from the probe data has been described elsewhere[14], and follows the techniques

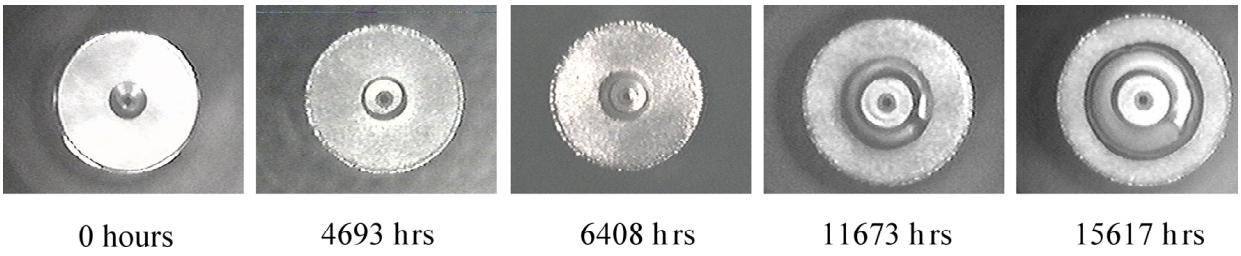

Figure 7. Photo of the NSTAR cathode evolution in the ELT test where the keeper electrode completed eroded out beyond the cathode diameter in 15,000 hours.

described by Chen[18]. The plasma density inside the NSTAR cathode is very high, and typically exceeds 10^{15} cm^{-3}, as shown in Fig. 8, for all but the lowest throttle points. In changing operating conditions from TH8 to TH15, which increases both the discharge current and flow rate, the density profile is shifted downstream toward the orifice, as also shown in Fig. 8. The neutral pressure inside the cathode for TH15 is on the order of 8 to 9 Torr, and is about 1.7 times that of TH8. Higher neutral pressures in the insert region are observed to push the peak density downstream and cause the cathode plasma density to fall more rapidly upstream from the orifice. This reduces the already small contact area between the plasma and the emitting insert surface. The plasma is in contact with the insert typically less than about 3 mm for this cathode, suggesting that cathodes with pressures approaching 5 to 10 Torr may only utilize a fraction of the insert length for any significant electron emission.[14] The probe signals for the TH8 case are typically observed to be much nosier than those for the TH15 case, which is related to large oscillations external to the cathode. It appears that the plasma in the cathode and keeper orifice regions for TH8 is inherently less stable than for TH15, probably due to the combination of gas flow and discharge current selected for this mode.

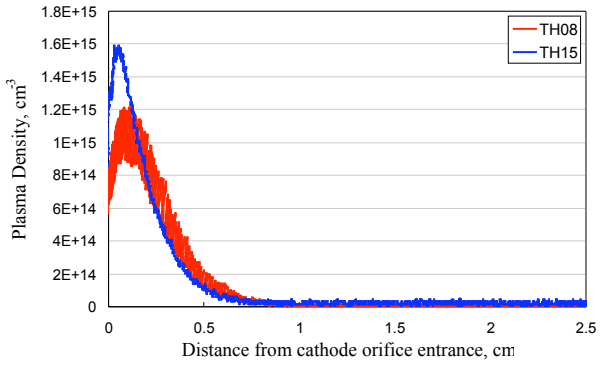

Figure 8. Cathode density profiles plotted on a linear scale for TH8 and TH15.

The axial plasma potential and electron

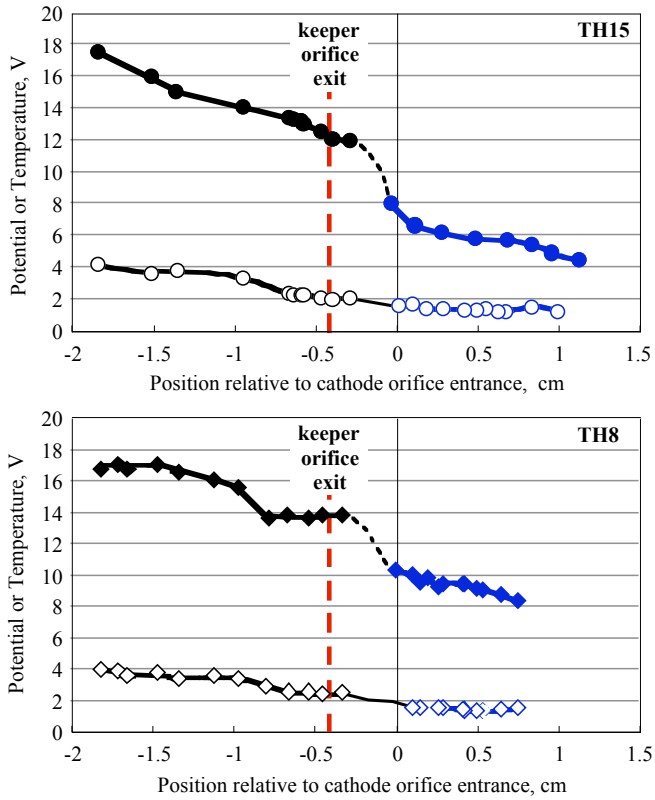

Figure 9. Plasma potential and electron temperature for the cathode-keeper region for TH15 (a) and TH8 (b).

temperatures measured through the hollow cathode plasma and into the keeper region are shown in Fig. 9 for the TH15 and TH8 modes. The 13-A TH15 mode shown in Fig.9a has a plasma potential inside the insert of about 6 V, while a higher 8 to 9 V potential is required the 8.2-A TH8 mode shown in Fig. 9b to self heat the cathode. The electron temperature in both cases is on the order of 1.5 V, and does not vary much over the throttle table due to the high pressures inside the insert region. The potential in the orifice region is difficult for the cathode-probe to measure because the probe ceramic cross sectional diameter is about half the orifice diameter, and the discharge is significantly perturbed by inserting the probe deep into the orifice. However, inserting the probe from the downstream anode side can penetrate inside the keeper orifice within a couple of millimeters of the cathode orifice without significantly altering the discharge. We see that the potential has jumped to the order of 12 to 14 V, and then increases slowly as the probes moves away from the keeper orifice. The axial potential is found to reach the about the anode potential within 10 cm of the cathode.

The plasma density and potential profiles downstream of the keeper electrode in the NSTAR geometry have been extensively measured with scanning probes by Herman and Gallimore[19], Jameson, et al.[15], and by Sengupta, et al.[20], and their results are consistent with our data when our probes are configured to measure the time-averaged plasma parameters. An example of the radial plasma potential profile measured by our radially scanning emissive probe positioned about 2 mm downstream of the keeper for TH15 is shown in Fig. 10. In this case, the data acquisition system is averaging the data at about 1 kHz, so this data represents the time-average radial potential profile. We see that the plasma potential is about 12 V on axis, in agreement with the anode probe data in Fig. 9a. The potential is a minimum on axis and increases to above the anode potential a distance of about 1 cm radially from the axis. Similar profiles extend axially such that the cathode plume forms a potential trough, with the potential increasing radially and axially from the keeper orifice. This of course is inverse to the plasma density profiles, which are peaked near the orifice and decrease radially and axially away from the keeper.

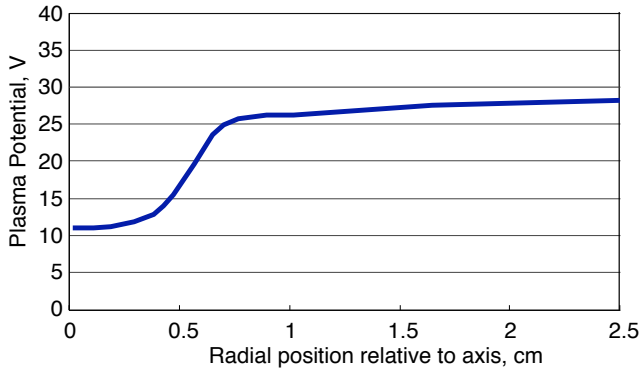

Figure 10. Time averaged radial profile of the plasma potential for TH15 operation from an emissive probe.

The plasma data indicates that the time-averaged plasma potential in the immediate keeper region is actually about the lowest found in the entire discharge chamber. The plasma density decreases monotonically from the keeper region both axially and radially, and electron temperature is relatively flat. Primary electrons, which will not be discussed in detail in this paper, have a relatively low energy (<15 V), and do not drive unusual density or potential structures around the keeper. The potential structure actually forms a trough leading back into the keeper orifice, and not the potential hill theorized to produce high-energy ions. Ions born in this region, from a DC potential sense, will tend to bombard the keeper and cathode with very low energy (<20 V), which will not cause the

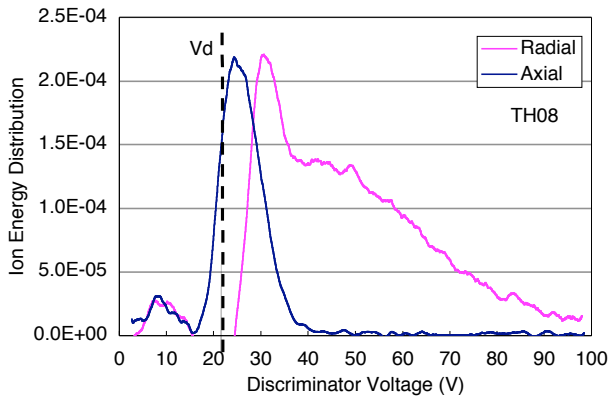

Figure 12. Ion energy distributions radially and axially for throttle level TH8.

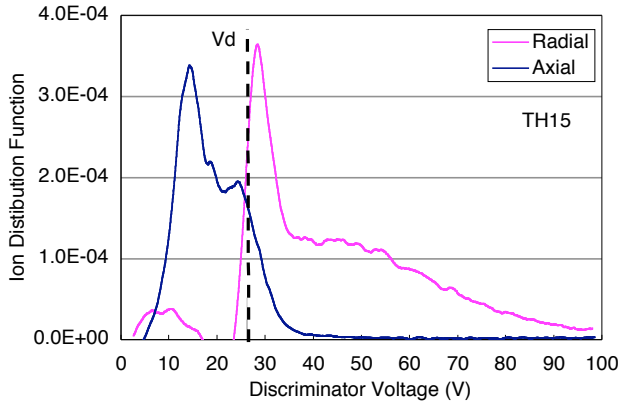

Figure 11. Ion energy distributions radially and axially for throttle level TH15.

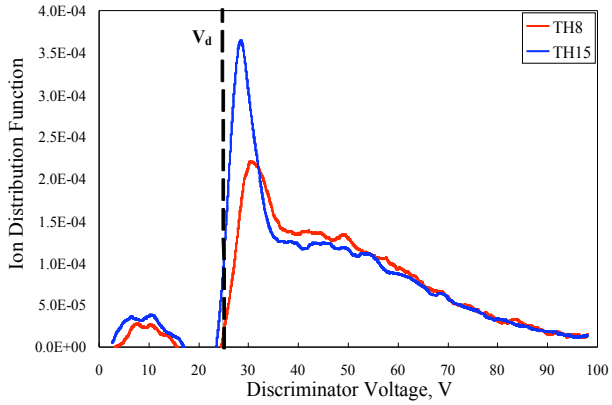

Figure 13. Comparison of radial ion energy distributions for TH8 and TH15 throttle points.

erosion rates or patterns observed in the experiments.

B. Ion Energy Measurements

To further analyze the keeper erosion mechanisms, a retarding potential analyzer (RPA) was placed both on axis and radially in the gap between the keeper and the anode to diagnose the ion energy distributions. The ion energy distributions measured in the axial and radial directions from the RPA in the TH15 mode are shown in Fig. 11. The axial measurements were taken with the RPA place 25 cm downstream of the cathode exit, while the radial measurements were taken with the RPA positioned directly in front of the keeper electrode, as shown in Fig. 4. The axial distribution has a peak at the discharge voltage, and a larger peak observed at a lower potential. Since the RPA only collects ions falling in the range from the plasma potential peak to the grounded analyzer, there are many ions born on the downward slope between the axial potential peak at the discharge voltage and the RPA that fall into the analyzer. Significantly, there are essentially no ions with energies in excess of 35 V measured on axis. This is consistent with measurements made elsewhere[21,22]. The ion distribution measured in the radial direction has a peak slightly above the anode voltage, corresponding to ions born off axis at the plasma potential above the anode voltage as shown in Fig. 10. However, the radial ion energy distribution shows there a large number of ions with energy significantly higher than the discharge voltage and extending out beyond 100 V. These ions certainly have sufficient energy to cause keeper erosion, and are produced in the region just downstream of the keeper electrode where the radially-oriented analyzer is collecting.

The ion energy distribution in the axial and radial directions for the TH8 throttle point are shown in Fig. 12. The axial distribution shows the typical peak at about the discharge voltage, and essentially no ions with energy in excess of 40 volts. The axial ion energy is again a result of the ions coming from the potential at which they were created, downstream of the potential peak, and falling into the cathode-potential analyzer. An analysis of the sputtering rate of the cathode and keeper orifices indicates that ions with nearly twice this energy would be required to produce the observed erosion rates in the ion thruster tests[18]. The radial ion distribution, on the other hand, shows a significant number of ions at energies well above the peak near the anode voltage and extending out to 100 V, similar to the TH15 results.

A direct comparison of the two radial ion energy distributions for TH8 and TH15 is shown in Fig. 13. The number of ions in the peak just above the anode voltage is larger for the TH15 case because the plasma density is about twice as high in this case compared to the TH8 case. However, the TH8 case appears to have a comparable number of high-energy ions, which is remarkable since the density is half of the TH15 case. The comparable number of high-energy ions in the two cases suggest that the keeper erosion in the ELT test in the TH8 mode should have been comparable to the TH15 mode. Since comparable erosion rates were not observed[10, 16], and the erosion pattern inferred from the life-test data is different, an alternative mechanism must be pursued. This mechanism must account for the fact that the TH15 erosion was largely to the keeper face (axial) and the TH8 erosion was largely radial in that the keeper orifice diameter increased with time as seen in Fig. 7. The axial erosion problem can be mitigated by manufacturing the keeper face plate out of a different material with a lower sputtering yield and by making the plate significantly thicker; hence tantalum and graphite keepers have been suggested for future missions using the NSTAR thrusters. However, no mechanism or solution for the radial erosion problem has been found other than utilizing a lower sputtering yield material like graphite or tantalum for the keeper material, which has a finite capability in increasing the keeper life related to the magnitude of the reduction of the sputtering yield compared to the NSTAR molybdenum keeper.

To address erosion pattern issue, the source of the high-energy ions flowing in the radial direction for both throttle levels was pursued. Since the ions fall from the potential at which they are created, there is no mechanism for the observed high ion energies reported in the literature in the DC-averaged potential profiles we measure (Fig. 10) and that are found in the literature[18,19]. However, if the plasma potential is oscillating, the ions can be created at a higher potential and gain sufficient energy falling to the keeper voltage to sputter the keeper at high rates. The rf oscillation of the plasma potential in the cathode plume was examined with the transverse emissive probe operated in the emission limited mode[23]. In this mode, the probe filament is heated to a sufficient temperature to emit electrons at the random plasma electron flux (or higher), and the probe thereby floats at the local plasma potential. A high impedance circuit (>10^8 Ω) capable of detecting up to 1 MHz oscillations was design and used to measure the plasma potential fluctuation profile radially in front of the keeper face plate.

Figure 14 shows the radial profile of the plasma potential from the rf-emissive probe at a distance of 2 mm downstream of the keeper for TH15. The white line in the figure is the average plasma potential for the fluctuations measured by the radial scan. This data again shows that the average plasma potential has a minimum on axis at 12-13 V, in agreement with the data-acquisition-averaged results in Fig. 8. As the emissive probe moves radially outward, the plasma potential increases significantly to above the discharge voltage all along the keeper face, and eventually decreases back to the anode potential near the anode wall (beyond this scan). The potential oscillations in the keeper region were found to be between 50-500 kHz, depending specifically on the operating conditions. The potential fluctuations in TH15 range from ±5 near the axis to ±20 V, with the largest fluctuations starting at about 6 mm from the axis out to 10 mm. Since the fluctuation levels approach 5 to 10 times the local electron temperature with a frequency of under 1 MHz, these oscillations are likely turbulent ion acoustic waves. The high frequency fluctuations are observed all along the radial scan, but are found to die out as the probe is positioned axially farther downstream in the cathode plume, and are not observed beyond 5-to-10 cm downstream of the cathode.

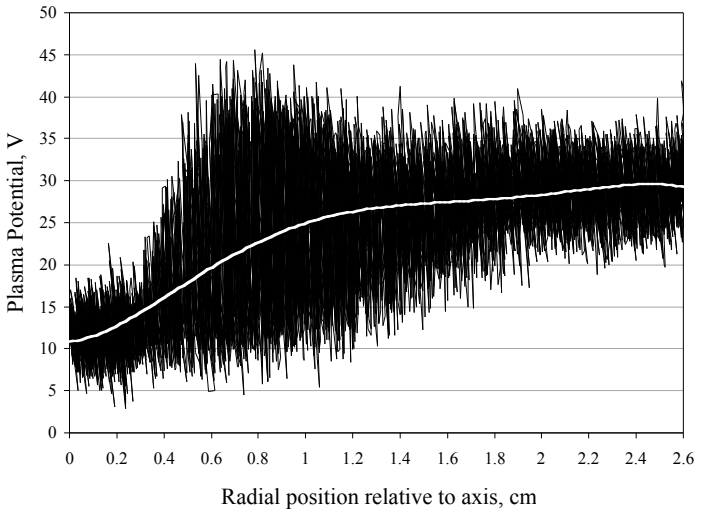

Figure 14. Plasma potential as a function of radius from the axis from the emissive probe for TH15, showing large amplitude oscillations in the frequency range of 50 to 500 kHz.

In hollow cathode discharges, there is typically a bright plasma "spot" or "ball" that is present in front of the keeper orifice. A series of photographs of the plasma ball are shown in Fig. 15 for several cases from TH15 through TH8. In the TH15 mode, this plasma ball can be clearly seen in Fig. 15(a) and extends from the keeper orifice to about 1 cm downstream into the anode plasma. The plasma ball also has a radial extent of less than 1 cm. The large

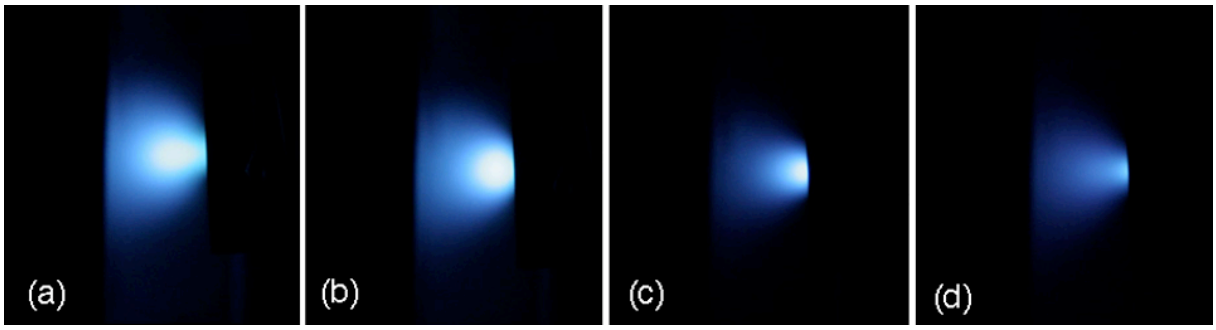

Figure 15. Photos of the plasma ball at the keeper exit for TH15 (a), TH12 (b), TH8 (c), and TH4 (d).

amplitude oscillations are observed to start at the edge of the ball, as seen in Fig. 14. As the discharge is operated at lower throttle levels, the plasma-ball is observed in Fig. 15 to be pulled back into the keeper. During the TH8 mode of interest, the ball is partially inside the keeper and just tail end of the ball can be seen at the downstream end of the keeper orifice, as seen in Figure 15(c). This suggests that the rapid radial keeper erosion observed during TH8 is a result of radially accelerated high energy ions from turbulent ion acoustic waves at the edge of the plasma ball striking the front corner and inside diameter of the keeper orifice. In the TH15 mode, the plasma ball is significantly outside of the keeper orifice, and the majority of these radially-accelerated ions miss the keeper. Ions born in the TH15 mode several millimeters off axis in the large fluctuation region can backstream to the keeper, resulting in the off-axis erosion ring observed in Fig. 6.

IV. NEXIS Cathode Results

To examine the keeper erosion mechanisms scaling with cathode size and provide a detailed study of the oscillations, a NEXIS 1.5-cm-dia. thermionic hollow cathode with a 0.25-cm-dia. orifice was installed in the system. The magnetic field configuration was identical to the NSTAR case, except that the axial field at the cathode orifice was reduce to about 80 G consistent with the NEXIS thruster operation. Figure 16 shows axial plasma density profile measured through the system at 25 A of discharge and 5.5 sccm xenon flow. We see that the density inside the hollow cathode is in the low 10^{14} cm^{-3} range, and falls from there into the to nominally around 10^{13} cm^{-3} in the keeper region and below 10^{12} cm^{-3} in the anode region. The transverse plasma density profiles for different axial positions from the keeper exit are shown in Fig. 17. The radial density profiles for the case of zero applied magnetic field is shown in Fig. 17a, and the nominal NEXIS discharge case of 80 G applied at the cathode is shown

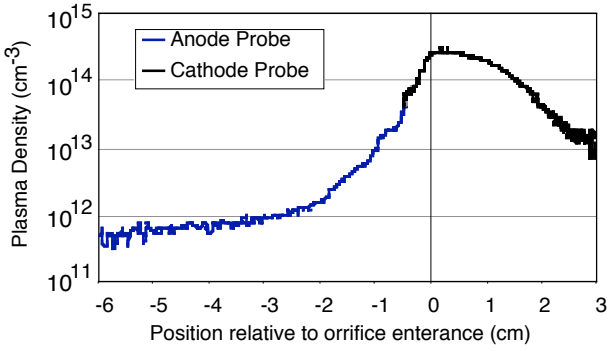

Figure 16. Axial plasma density profile for the NEXIS cathode operating at 25 A and 5.5 sccm flow.

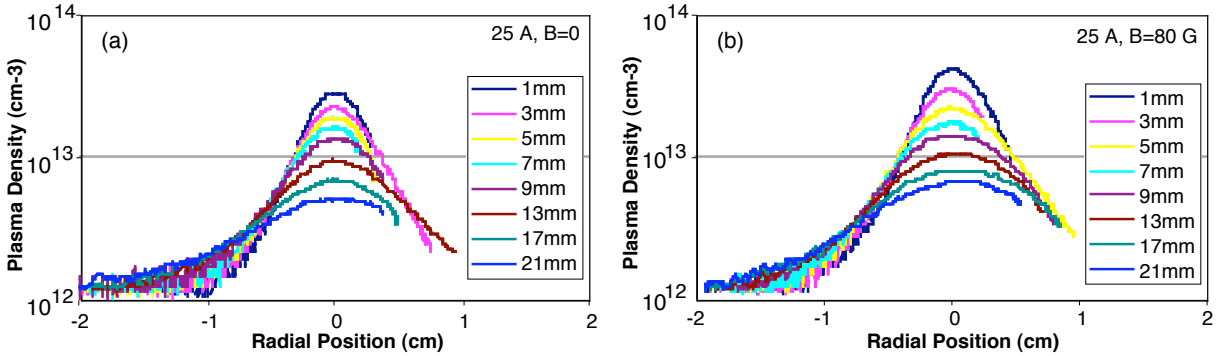

Figure 17. Radial density profiles for the NEXIS cathode for two cases of applied cathode magnetic field.

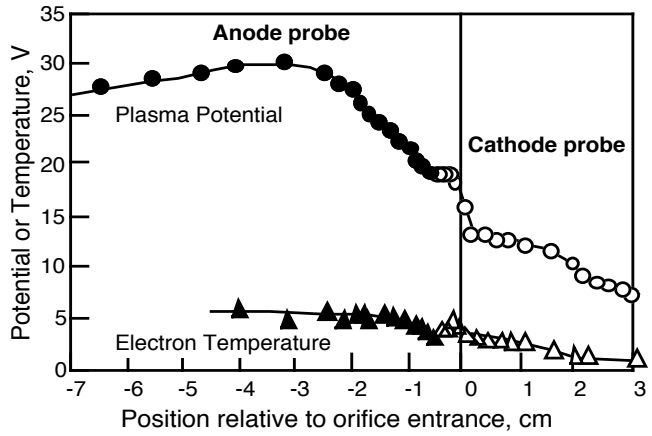

Figure 18. Plasma potential and temperature profiles for the 25 A, 5.5 sccm case.

in Fig. 17b. We see that the plasma density in the plume at any given distance from the cathode is about 50% higher with the applied magnetic field due to the confinement of the plasma and primary electrons. As with the NSTAR cathode, the plasma density is the highest on axis and near the cathode, and the cathode plume disperses radially with axial distance from the keeper.

The typical plasma potential and electron temperature profiles measured by the axially scanning probes are shown in Fig. 18 for the same discharge case. At the standard 1-kHz voltage sweep rate used in these experiments and the 1–m/sec probe-scanning speed, the data points in Fig. 18 have a position resolution of about 0.05 cm. While the data acquisition system samples at a rate of 300 kHz/channel, the frequency response of the these parameters represent time-averaged values Langmuir probe circuits is only about 50 kHz. Therefore, compared to the high frequency oscillations observed in Fig. 14.

Inside the hollow cathode, the plasma potential for our nominal discharge conditions is about 12 V above the cathode potential, consistent with the desire to obtain a reduction in the ion energy bombarding the low work-function electron emitting surface and preserve the low work function barium-oxide surface. Inside the cathode orifice, a potential discontinuity or double layer with a magnitude of less than 10 V is observed. The plasma potential is essentially flat through the keeper region, and then increases slowly to a peak of about 30 V (about 5 V above the anode potential) several cm downstream of the cathode. The electron temperature is several eV inside the cathode, increasing up to 5 eV in the downstream cathode plume.

Figure 19a shows the ion energy distribution from the RPA for various discharge currents at a constant xenon gas flow with the RPA facing directly on axis at the cathode and positioned 25-cm downstream. The RPA discriminator grid was swept at a frequency of 10 Hz during these experiments, so this data represents the time averaged DC ion energy distributions. The ion energy is again a result of the ions falling from the potential at which they were created into the cathode-potential analyzer. The axial data shows a broad distribution of ion energies from ions created at plasma potentials from several eV above cathode potential up to several eV above the discharge voltage. The maximum ion energy measured in this orientation increases slightly with discharge current to on the order of about 40 eV, which is consistent with the ion energies measured on axis in other experiments[20]. As mentioned above, ions with nearly twice this energy would be required to produce the observed erosion rates in the ion thruster tests[8-10].

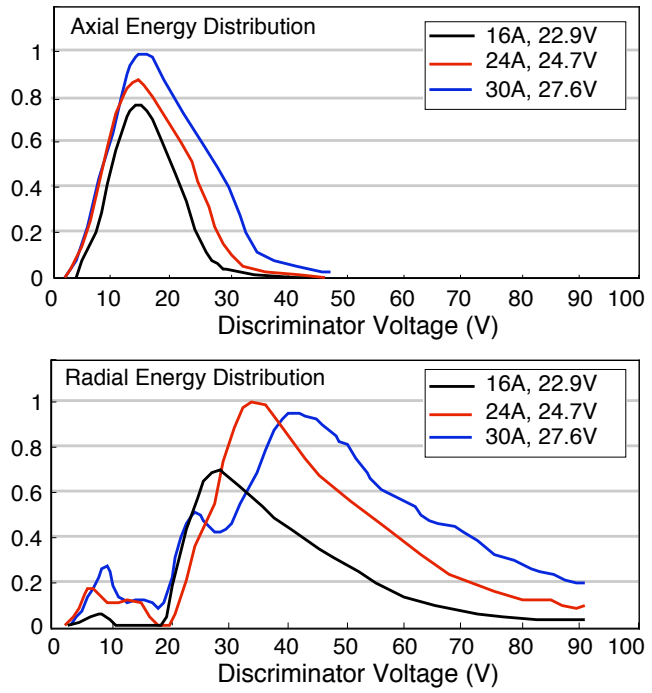

Figure 19. Axially oriented (a) and radially oriented (b) RPA data.

Figure 19b shows the ion distribution functions for the same discharge cases as in (a) but measured with the RPA positioned immediately downstream of the cathode keeper exit and oriented radially from the cathode plume (as in Fig 4). In this orientation, the RPA detects ions with energies starting at about the discharge voltage and extending to values well in excess of 100 eV. These ions are energetic enough to cause the significant keeper and anode wall erosion from sputtering reported in the literature. The high-

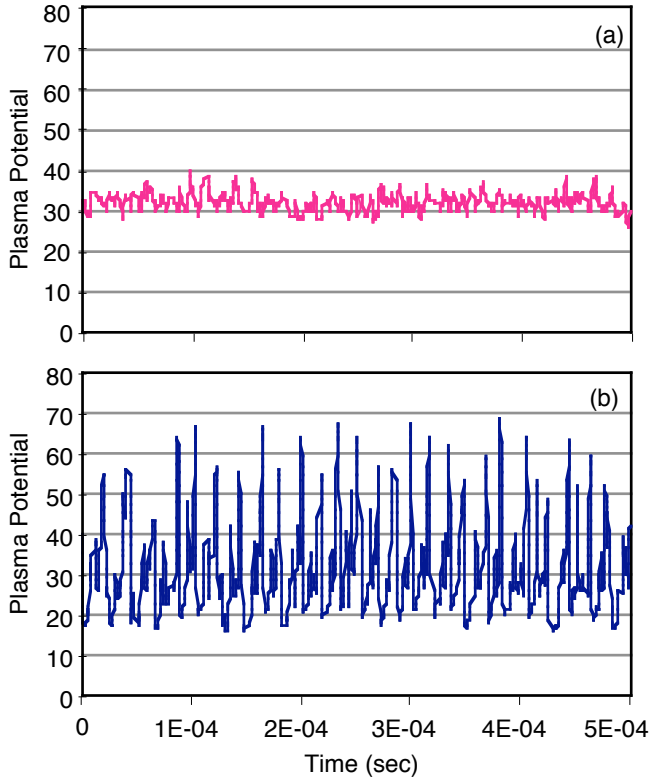

Figure 20. Plasma potential oscillations measured at the edge of plasma ball for 25 A for 80 G (a) and 10 G (b).

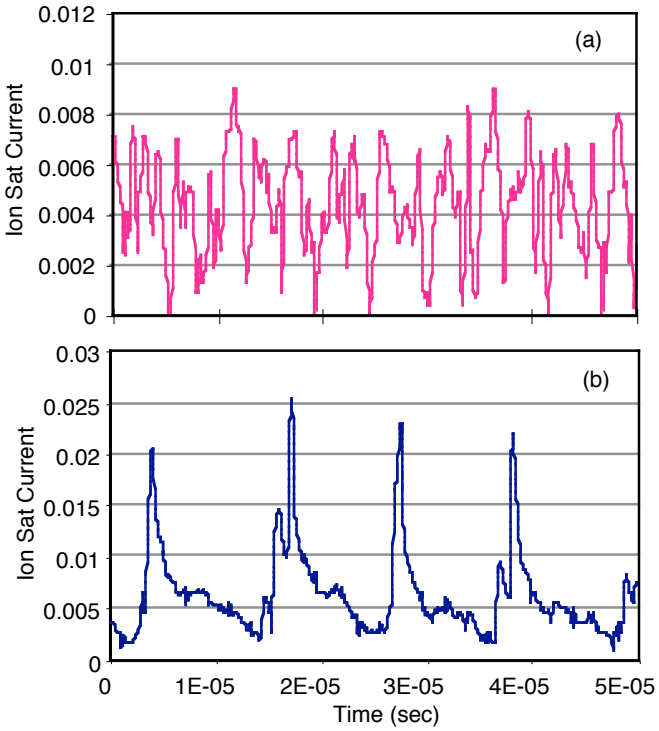

Figure 21. Ion saturation oscillations at edge of plasma ball for 25 A at 5.5 sccm (a) and 4 sccm (b). Note time scale is diffrent than in Fig. 20.

energy ion tail found in the radial direction from the cathode plume is consistent with measurements at other laboratories of higher energy ions detected in the downstream region of the thruster, but measured off-axis from the cathode[3,20].

As with the NSTASR cathode, there is clearly no DC potential hill keeper exit as shown in Fig. 18, such as was proposed in Ref. 13, at or near the cathode orifice that could produce the energetic ions observed by the radial RPA. The axial RPA data is consistent with ions generated downstream of the gradual potential peak that exists several cm downstream of the cathode and falling into the analyzer, while the radial RPA data cannot be explained by these DC potential profiles.

It has also been proposed[2] that plasma instabilities in the double layer inside the cathode orifice can accelerate ions to high energy. Recent theoretical modeling[24] of the plasma region inside the cathode suggested that turbulence near the orifice entrance may develop as a result of wave growth from streaming electrons and ions, which are subject to reduced Landau damping due to the relatively low ion-to-electron temperature ratio (~0.1). However, these calculations only extended up to the orifice entrance where turbulent heating is likely due to the increasing electron current densities entering the orifice. To investigate proposed oscillations in the cathode interior or orifice region, the scanning probes were biased to ion saturation and connected to a 1-Gbs digital oscilloscope. Inside the cathode orifice, ion-acoustic type oscillations on the order of 1 MHz were detected, but were found to be very small in amplitude ($\delta n/n \approx 1\%$). There were no significant oscillations detected inside the hollow cathode or in the cathode orifice region for the NEXIS cathode.

However, when the probes were scanned into the bright "plasma ball" characteristically observed outside the cathode and keeper regions, strong potential and density oscillations were again detected as with the NSTAR cathode. The transverse scanning probe was again configured as an emissive probe that is operates sufficiently hot to float at the plasma potential[23]. The high-impedance (>100 MΩ) voltage detection circuitry used to measure the DC and rf plasma potential is sensitive to voltage fluctuations of up to 1 MHz at peak voltages of up to 80 V. Figure 20 shows the plasma potential measured with the emissive probe at the edge of the plasma ball for two

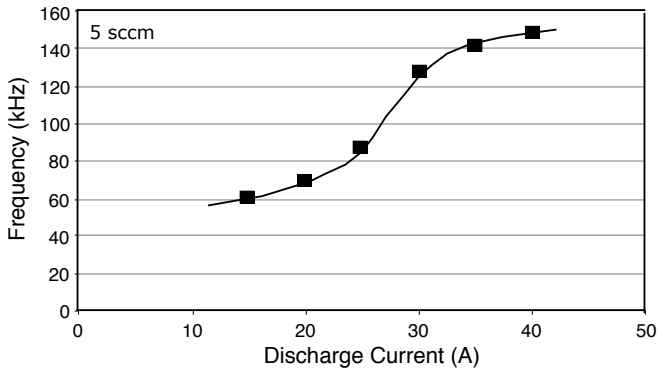

Figure 22. Frequency dependence on discharge current for the low frequency oscillations.

applied magnetic fields at the cathode. As the applied magnetic field is reduced, as shown the figure, or as the gas flow is reduced, the discharge breaks into high amplitude potential oscillations exceeding a peak potential of 70 V. The density in the case of Fig. 20a where the potential is rather quiet fluctuates significantly. Figure 21a shows the fluctuation in the ion saturation current (on a faster time scale compared to Fig. 20) measured by the transversely scanning probe inserted into the edge of the plasma ball for the nominal 25 A, 5.5 sccm case. The oscillations are relatively incoherent with frequencies of 0.5 to 2 MHz and amplitudes up to 100 percent of the ion saturation current. Reducing the gas flow rate, as shown in Fig. 21b, causes the oscillations to change into ≈100 kHz large-amplitude spikes characteristic of what we call "predator-prey" oscillations[25]. These oscillations are at the same frequency as the potential oscillations observed in Fig. 20b, and are related to an ionization instability caused by burning up the gas locally in the cathode plume. Transition of the oscillations from the high frequency incoherent fluctuations to the low frequency "predator-prey" oscillations could also be achieved by lowering the applied magnetic field at the cathode exit, which affects the plasma production in this region in a similar manner as reducing the cathode gas flow. The predator-prey-type oscillations were observed to increase in frequency and amplitude as the discharge current increased, as shown in Fig. 22, and increased in amplitude as the gas flow decreased. The oscillations appear to be precursors to larger amplitude "plume-mode" oscillations[26] that appear in the discharge voltage and keeper potential at similar frequencies. The transition from incoherent fluctuations to predator-prey type oscillations depends on the discharge current, gas flow rate, and magnetic field, and both types of behavior could be observed over large ranges in the discharge parameters.

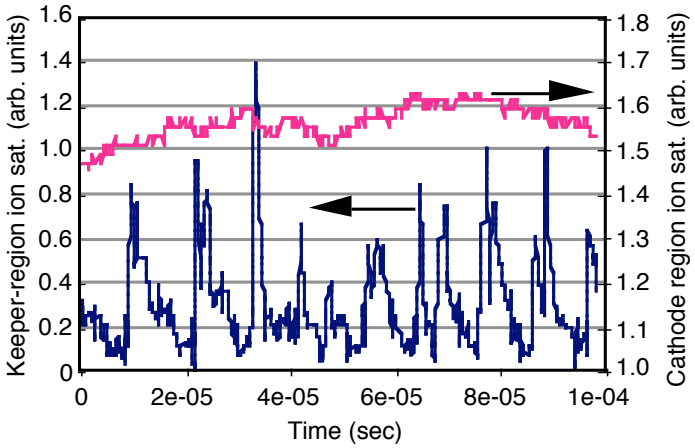

Figure 23. Ion saturation current inside and outside cathode showing no correlation to the oscillations in the hollow cathode insert plasma.

Experiments determined that the density oscillations shown in Fig. 22 in the plasma ball density do not extend into the interior of the hollow cathode plasma. Figure 23 shows the ion saturation current measured simultaneously by the transverse scanning probe in the plasma ball outside of the cathode and by the axially scanning probe located just upstream of the cathode orifice plate. There is no correlation to the signals, and the fluctuation level inside the hollow cathode is very low. This is very different than the case shown in Fig.8 for the NSTAR cathode where the oscillation appeared to couple into the cathode density. However, a careful investigation of this situation showed that extremely large predator-prey modes in the plasma ball region in the NSTAR cathode can trigger discharge power supply regulation oscillations. These ≤1 kHz discharge supply oscillations then modulate the discharge voltage and current, which appears in the plasma density. In Fig. 8, large predator-prey oscillations in the TH8 mode caused the discharge supply oscillation, but the predator prey modes in TH15 and in all cases with the NEXIS cathode were significantly smaller and did not trigger the power supply regulation problem.

It appears that there are three classes of oscillation in these discharges: 1) high frequency (0.1-1 MHz) turbulent ion acoustic oscillations, 2) medium frequency (40-100 kHz) predator-prey ionization instability oscillations, and 3) low frequency (≤1 kHz) discharge power supply regulation oscillations. The high frequency ion acoustic oscillations are always present, and can be detected in the cathode orifice and keeper regions. The lower frequency oscillations occur in special cases of orifice size, discharge current and cathode gas flow rate.

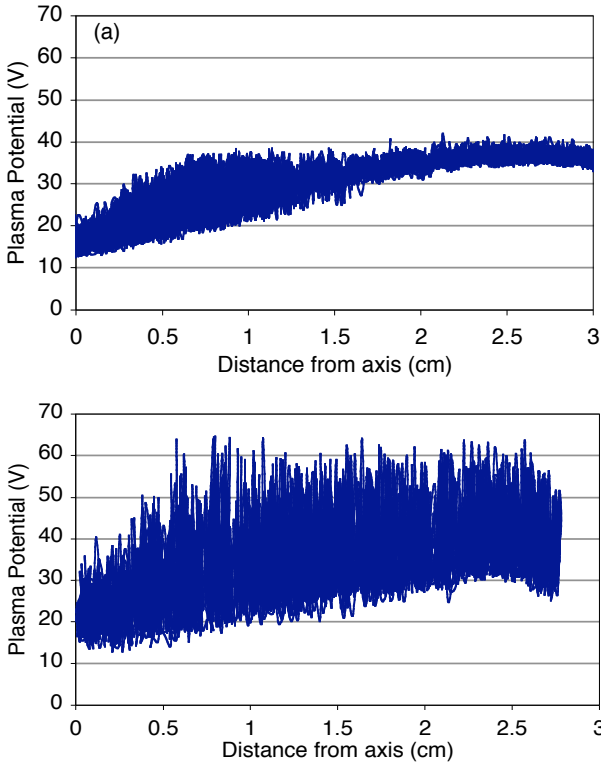

Figure 24. Radial plasma potential profiles at 25 A for 5.5 sccm (a) and 4 sccm (b).

Figure 24 shows the radial profile of the rf plasma potentials from the scanning emissive probe for our nominal case of 25 A at 5.5 xenon flow at two values of the applied magnetic field at the cathode. For the nominal gas flow case of 5.5 sccm with 80 G applied, the potential on axis seen in Fig. 24 a is nominally about 18 V, which is consistent with the scanning Langmuir probe "time-averaged" data shown in Fig. 18. With the magnetic field turned down to 10 G or less, the frequency drops into the predator-prey mode shown in Fig. 24b, and the amplitude of the oscillations is consistent with the data shown in Fig. 20 at the edge of the ball. As in NSTAR, the average plasma potential profile forms a well or trough centered on the bright "plasma ball" observed on axis, consistent with the time-averaged emissive probe measurements presented in Refs. 16, 17 and 19. The potential increases radially over several cm to a peak of about 5 V in excess of the discharge voltage and then extends at about that potential to near the anode surface. If the gas flow is decreased as in Fig. 24b, or the applied magnetic field at the cathode is decreased, the plasma breaks into the large amplitude, 80-kHz oscillations seen in Fig. 21. The rf plasma potential has peak fluctuations in excess of 60 V starting at the edge of the ball and extending radially outward to the anode wall.

The ion current collected by the RPA was compared to the plasma density and potential fluctuations measured by the probes. Figure 25 shows the transverse Langmuir probe ion current fluctuations measured at the edge of the plasma ball, the RPA collector current and the AC component of the discharge voltage. While the probe and RPA current fluctuations are reasonably well correlated, these fluctuations are not driven by oscillations in the discharge voltage. The discharge voltage oscillations shown are typical of normal low frequency (≤1 kHz) power supply current regulation time constants. Figure 26a shows that the high frequency plasma potential oscillations are uncorrelated with the collected RPA current. However, the low frequency potential oscillations shown in Fig. 26b are well correlated to the measured RPA ion current, but about 180 degrees out of phase. This signal phasing is consistent with the ions being born at a high potential near the cathode and flowing to the RPA in bursts at the predator-prey oscillation frequency as the plasma density and potential collapses.

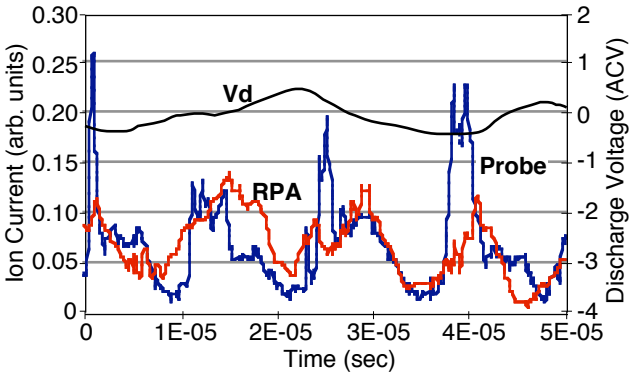

Figure 25. Ion current from scanning probe at the edge of the plasma ball, ion current collected by the RPA, and discharge voltage.

A direct comparison of the ion energies with and without the large amplitude oscillations was made using the radially-positioned RPA for the cases in Fig. 26, and the results shown in Figure 27. We see that the low magnetic field case (with the low frequency oscillations) produces significantly larger numbers of high-energy ions compared to the nominal case. It seems very likely that the amplitude of the plasma potential oscillations shown in Fig. 24 are directly related to the number of high-energy ions measured in the keeper region in Fig. 26. The mechanisms for accelerating the ions have not been directly determined at this time, but it is likely that any ions born at high potential during an oscillation will fall through the potential drop to the cathode potential RPA and gain that associated energy. This is also true for double ions, which will gain twice

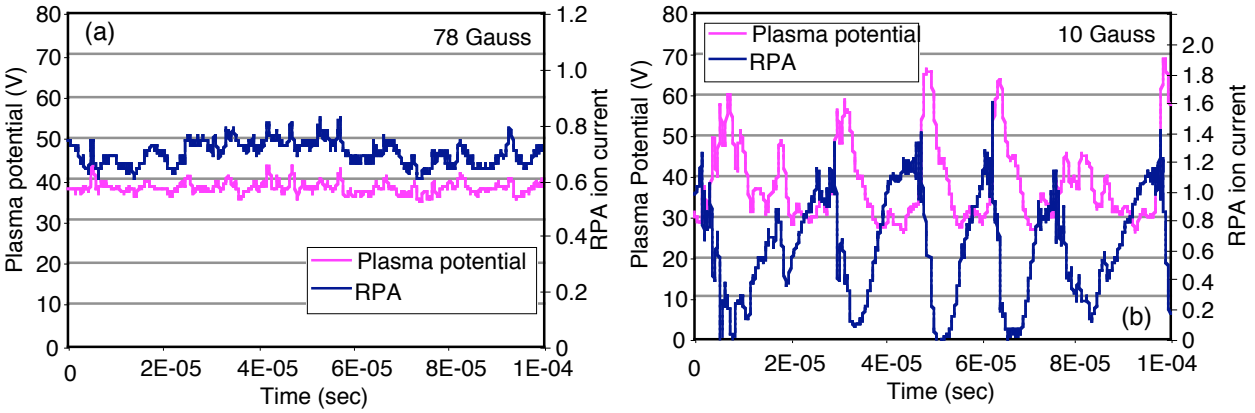

Figure 26. RPA current and plasma potential oscillations for two magnetic fields at 25 A and 5.5 sccm.

the energy falling through the same potential. Recent measurements at CSU indicate that the double ion content in the radial ion flux in front of the keeper can exceed 50% of the ion current[27], which at these high energies would represent a significant source of erosion. The fact that high energy ions are also observed (in reduced numbers) with only very high frequency oscillations (0.5-1 MHz) points to additional acceleration mechanisms such as turbulent ion acoustic transport. Theoretical and experimental investigations aimed at understanding the role of the ion acoustic waves in producing the high-energy ions are underway.

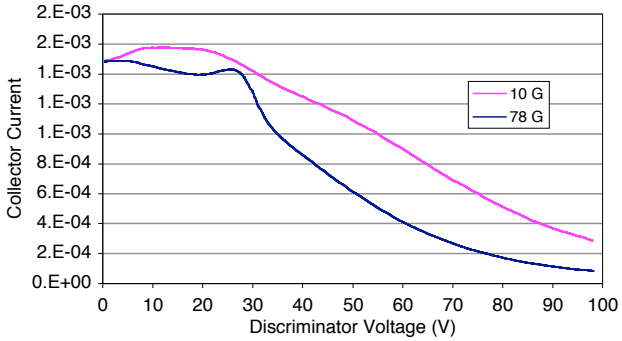

Figure 27. Comparison of RPA current for the case of low magnetic field (low frequency, large amplitude oscillations), and nominal magnetic field for the NEXIS cathode.

Finally, the axial location of the plasma ball in front of the large NEXIS cathode is also observed to change with the discharge parameters. It is generally observed that increases in gas flow, discharge current, and magnetic field all cause the plasma ball to move downstream. Increases in the gas flow generally reduce the observed oscillation level, especially of the low frequency predator-prey modes associated with collapse of the plasma due to burning up the gas in the cathode plume. Figure 28 shows photographs of the cathode plume for the NEXIS cathode for the nominal 25 A, 5.5 sccm condition (left) and a high

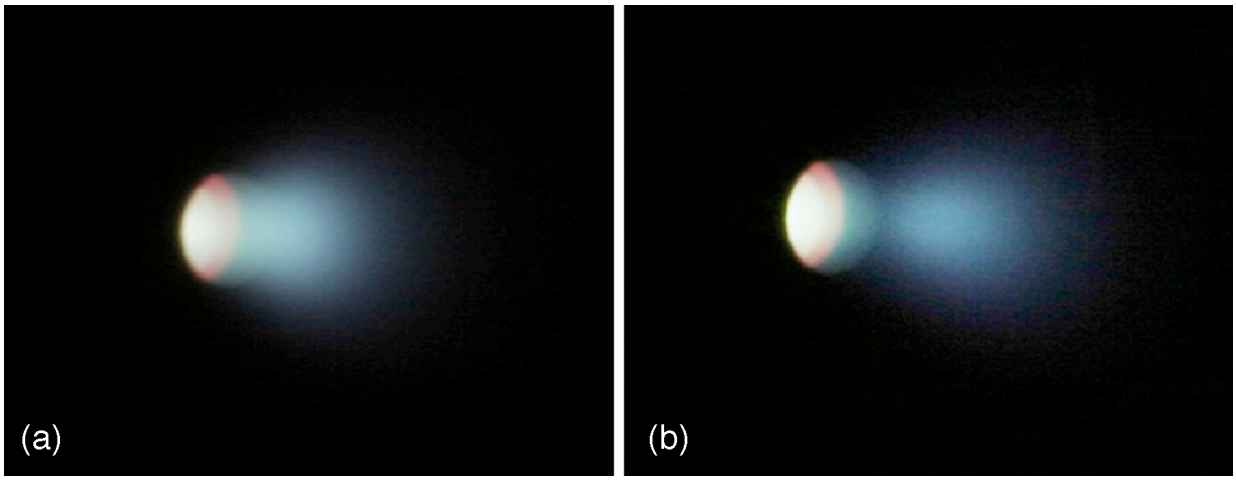

Figure 28. Plasma ball location for the nominal 25A, 5.5 sccm case (a) and a 25 A, 10 sccm case (b).

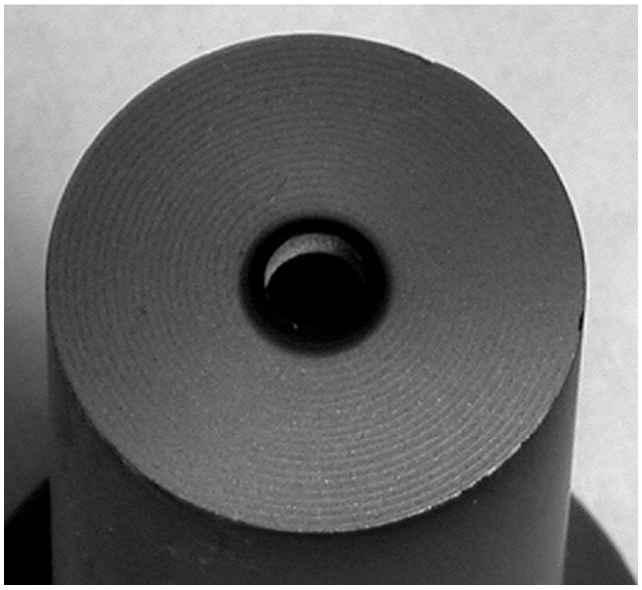

Figure 29. Photo of the NEXIS keeper face after the 2000 hour wear test.

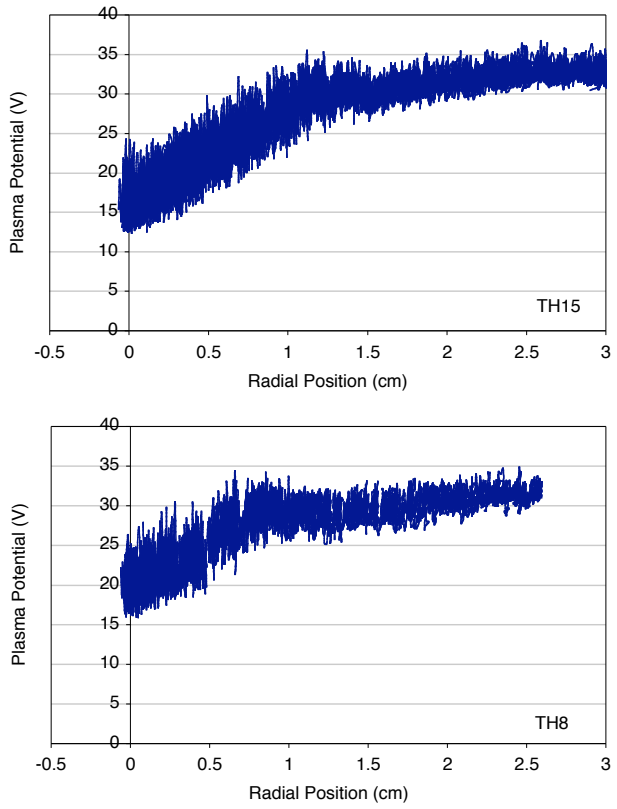

Figure 30. Radial plasma potential oscillations for the NSTAR cathode with the modified keeper at TH15 and TH8 showing oscillation suppression.

flow of 10 sccm case (right). The plasma ball moves significantly downstream at higher flow rates, and a dark space associated with very cold electron temperatures is observed to form between the cathode and the plasma ball. Probe measurements in the dark space region confirmed that the lowest electron temperatures occurred in this region, and the electron temperature increased as one moved downstream into the plasma ball. This suggests that the plasma ball is a structure intended to enhance the ionization in the cathode plume sufficiently to carry the discharge current from the keeper region into the anode region.

In both gas flow cases shown in Fig. 28, the plasma ball is located significantly downstream of the keeper orifice in the NEXIS cathode. Since the strong oscillations appear related to the plasma ball structure and are primarily detected at the radial edge of the ball, and the generation of the high energy ions is related to the potential fluctuations, it is expected that the NEXIS cathode will have low keeper wear rates because the plasma ball is much less coupled to the keeper than in the NSTAR geometry where in some throttle levels the ball is entirely inside the keeper orifice. In addition, since the amplitude of the oscillations increases with lower gas flow and the location of the source of the high energy ions moves toward the keeper as the gas flow decreases, higher keeper erosion is expected consistent be consistent with the higher keeper noise and currents reported when cathodes transition into the plume mode[26].

The NEXIS cathode was examined after a recent 2000 hour wear test[28] in the thruster at a nominal current of 27 A and a flow of 6.5 sccm. Careful laser-profilometry measurements indicated that the keeper face and orifice were essentially unchanged from the before-test inspection. Figure 29 is a photograph of the keeper face taken after the test, and shows a uniformly smooth keeper face surface with the exception of some light graphite soot around the orifice. This soot is very weakly bound, and is easily removed by any ion bombardment. The presence of this soot indicates that the keeper orifice region experienced little or no ion bombardment, and so should experience no wear. The smooth surface outside the soot is in contrast to the NSTAR cathode shown in Fig. 7, where the localized ion erosion pattern was evident. This behavior supports the cathode experiments described here that indicate that with the proper cathode/keeper design and with the proper selection of the cathode operating parameters, keeper wear can be mitigated.

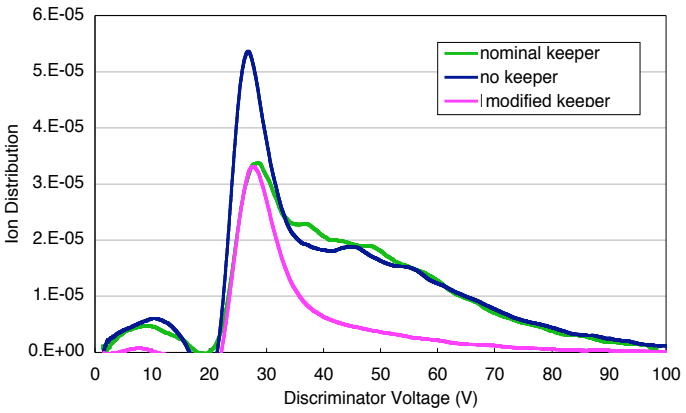

Figure 31. Ion energy distribution for NSTAR TH15 mode operation with the nominal keeper, no keeper, and a modified keeper.

V. High Energy Ion Suppression

An attempt was made to suppress the oscillations that lead to the high-energy ions observed in the hollow cathode tests. Since the oscillations appear to be related to either predator-prey modes or turbulent ion acoustic waves, both of which depend strongly on the local gas pressure and plasma temperatures, the keeper electrode was modified to change the geometry and the gas flow pattern at the exit. Figure 30 shows the radial plasma potential profile and oscillations for the NSTAR cathode operating at TH15 and TH8. The large amplitude plasma potential oscillations have been suppressed in both cases. Figure 31 shows the ion energy distribution measured with the radially-positioned RPA for the nominal keeper design, no keeper, and the modified keeper. We see that the keeper modification significantly reduced the high-energy ion tail compared to the nominal case. This is consistent with the suppression of the oscillations in Fig. 30. The lack of oscillations and the strong reduction in the magnitude of the high-energy ion tail is expected to significantly reduce the keeper erosion compared to the nominal geometry.

VI. Conclusion

An investigation of the plasma parameters in the cathode insert, keeper and anode regions of hollow cathodes used in NSTAR and NEXIS ion thrusters has been undertaken to determine the mechanisms high energy ion production and keeper erosion. The RPA analyzer showed few high energy ions directed in the downstream axial direction, but a significant number of ions with energies in excess of the discharge voltage and up to 100 eV were found to flow in the radial direction in front of the keeper. The presence of high energy ions in this location which can strike the keeper are consistent with erosion of the keeper face and orifice by sputtering. The erosion pattern observed on the NSTAR keeper face at TH15 suggests that the flux of high-energy ions is not purely radial, but has some component in the upstream and downstream axial directions. This is consistent with the detection of some number of high-energy ions off axis by other researchers, and the elongated shape of the plasma ball.

Detailed measurements of the potential distributions throughout the discharge could not find a DC mechanism for acceleration of ions to the high energies (>50 V) observed in these discharges under certain conditions. However, rf measurement of the plasma potential profile show fluctuations in the range of 50-500 kHz exist in the keeper region, with the largest amplitudes occurring at the edge of the plasma ball downstream of the cathode orifice in the keeper region. These oscillations range from ionization instabilities to turbulent ion acoustic waves, and can in some cases interact with the discharge power supply to cause gross unstable operation. The current of the high-energy ions collected by the RPA is consistent with the rf ion current and the large-amplitude potential fluctuations. The results shown here indicate that proper cathode/keeper design and proper selection of the cathode operating parameters, the plasma oscillations and high ion energies can be suppressed, which will reduce and hopefully mitigate excessive keeper wear.

Acknowledgments

The research described in this paper was carried out by the Jet Propulsion Laboratory, California Institute of Technology, under a contract with the National Aeronautics and Space Administration in support of Project Prometheus.

References

[1]A.T. Forrester, *Large Ion Beams*, Wiley-Interscience, NY, 1988.

[2]V.J. Friedly and P.J. Wilbur, "High current hollow cathode phenomena", J. Propulsion and Power, **8**, 635 (1992).

[3]I. Kameyama and P. Wilbur, "Measurement of ions from high current hollow cathodes using electrostatic energy analyzer", J. Propulsion and Power, **16**, 529 (2000).

[4]G. Williams, et al., "Laser induced fluorescence characterization of ions emitted from hollow cathodes", IEEE T-PS, **28**, 1664 (2000).

[5]J. Foster and M. Patterson, "Downstream ion energy distributions in a hollow cathode ring cusp discharge", J. Propulsion and Power, **21**, 144 (2005).

[6]M. Croften and I.Boyd, "Plume measurements and modeling results for a xenon hollow cathode", AIAA Paper 2002-4103, July 2002.

[7]J.R. Brophy and C.E. Gardner, "Tests of high current hollow cathodes for ion engines" AIAA Paper 88-2913, 24th joint Propulsion Conference, Boston, MA, July 11-14, 1988.

[8]M. Domonkos, J.Foster, G.Soulas, "Wear testing and analysis of ion engine discharge cathode keeper", J. Propulsion and Power, **21**, 102 (2005).

[9]J. Polk, et al., "An overview of the results of an 8200 hour wear test of an NSTAR ion thruster", AIAA Paper 1999-2446, 35th Joint Propulsion Conference, Los Angeles, CA, June 20-24, 1999.

[10]A. Sengupta, et al., "An overview of the results from the 30,000 hours life test of Deep Space 1 flight spare engine", AIAA Paper 2004-3608, 40th Joint Propulsion Conference, Ft. Lauderdale, FL, July 11-14, 2004.

[11]M.Patterson, et al., "2.3 kW ion thruster wear test", AIAA Paper 95-2516, 31th Joint Propulsion Conference, July 1995.

[12]J.R. Brophy, "NASA's Deep Space 1 ion engine", Rev.Sci.Instrum. **73**, 1071 (2002).

[13]I. Kameyama, P.Wilbur, "Potential hill model of high energy ion production near hollow cathodes", ISTS Paper #98-a-2-17, 21st Intl. Symp. Space Tech. Sci., Sonic City, Omiya, Japan, May 24-21, 1998.

[14]D.M. Goebel, K. Jameson, R. Watkins, I. Katz, "Hollow Cathode and Keeper-Region Plasma Measurements Using Ultra-Fast Miniature Scanning Probes "AIAA Paper 2004-3430, 40th Joint Propulsion Conference, Ft. Lauderdale, FL, July 11-14, 2004.

[15]K. Jameson, D.M. Goebel, R. Watkins, "Hollow cathode and keeper region plasma measurements", AIAA Paper 2005-3667, 41th Joint Propulsion Conference, Tucson, AZ July 11-13, 2005.

[16]R. Kolasinski and J. Polk, "Characterization of keeper wear by surface layer activation", AIAA Paper 2003-5144, 39th Joint Propulsion Conference, Huntsville, AL, July 20-23, 2003.

[17]J.E. Polk, D.M. Goebel, J.S. Snyder, et al., "Performance and wear test results for a 20-kW class ion engine with carbon-carbon grids", AIAA Paper 2005-4393, 41th Joint Propulsion Conference, Tucson, AZ July 11-13, 2005.

[18]F. Chen, in *Plasma Diagnostics Techniques*, Academic Press, NY, p.113-200 (1966).

[19]D. Herman and A. Gallimore, "Near discharge cathode assembly plasma potential measurements in a 30-cm NSTAR type ion Engine", AIAA Paper 2004-3958, 40th Joint Propulsion Conference, Ft. Lauderdale, FL, July 11-14, 2004.

[20]A. Sengupta, "Experimental investigation of discharge plasma magnetic field confinement in an NSTAR thruster", AIAA Paper 2005-4069, 41th Joint Propulsion Conference, Tucson, AZ July 11-13, 2005.

[21]C. Farnell and J. Williams, "Characteristics of energetic ions from hollow cathodes", IEPC Paper 03-072, 28th International Electric Propulsion Conference, Toulouse, France, March 17-21, 2003.

[22]C. Farnell and J. Williams, "Measurements of ion energy distributions produced within n NSTASR discharge chamber", AIAA Paper 2004-3432, 40th Joint Propulsion Conference, Ft. Lauderdale, FL, July 11-14, 2004.

[23]N.Hershkowitz and M Cho, "Measurement of plasma potential by electron emissive probes", J. Vac.Sci Tech. **A**, 2054 (1988).

[24]I. Mikellides, I.Katz, D. Goebel, J. Polk, "Theoretical model of a hollow cathode insert plasma", AIAA Paper 2004-3817, 40th Joint Propulsion Conference, Ft. Lauderdale, FL, July 11-14, 2004.

[25]J.P. Boeuf, and L. Garrigues,, "Low frequency oscillations in a stationary plasma thruster", J. of Appl. Phys., Vol. 84, 3541-3554, 1998.

[26]T.M. Jack, S.W. Patterson and D.G. Fearn, "The effect of the keeper electrode on hollow cathode discharge characteristics", AIAA paper 2000-3533, 36th Joint Propulsion Conference, July 2000.

[27]J. Williams, et al., "Correlation of remote and direct measurements of plasma properties generated within the discharge chamber of an NSTAR thruster" IEPC 2005-294, International Electric Propulsion Conference, Princeton, NJ, Oct.31st-Nov.4th, 2005.

[28]J.S. Snyder, D.M. Goebel, J.E. Polk, and A.C. Schneider, "Results of a 2000-hour wear test of the NEXIS ion engine", IEPC 2005-281, International Electric Propulsion Conference, Princeton, NJ, Oct.31st-Nov.4th, 2005.